INSTRUMENTAL COMPLEX AND THE RESULTS OF PRECISE MEASUREMENTS OF MILLIMETER- AND SUBMILLIMETER-WAVE PROPAGATION IN CONDENSED MEDIA AND THE ATMOSPHERE

V. V. Parshin, M. Yu. Tretyakov,* M. A. Koshelev, and E. A. Serov

UDC 537.86

We describe an instrumental complex based on high-Q open Fabry–Perot resonators for the frequency band 36–370 GHz and present original measurement techniques and the latest results of measuring (i) refractive indices and losses of modern high-quality dielectrics for high-power electronics (with prognosis for up to the terahertz band) and general-purpose dielectrics including films, (ii) reflectivities of both antenna reflectors of cryogenic-receiver radiotelescopes and the so-called "hot" antennas for future Mercurian missions, and (iii) the atmospheric absorption for the development of high-precision wave-propagation models including the continuum absorption. The instrumentation and the measurement techniques are intended for studying condensed-media parameters at temperatures 80–900 K and atmospheric parameters at temperatures from $-40\,^\circ C$ to $+60\,^\circ C$ and humidities from 0 to 80%.

1. INTRODUCTION

In this work, we describe an instrumental complex based on high-Q open Fabry–Perot resonators for studying gases and condensed media at frequencies 36–370 GHz and temperatures 80–900 K. Attention is focused on the state-of-the-art measurement techniques which improved the dielectric-constant measurement accuracy and confidence by more than an order of magnitude.

The results of studying the refractive indices n and losses (the loss tangents $\tan\delta$) of both modern high-quality ultralow-loss dielectrics for high-power electronics and general-purpose dielectrics including polymers are presented.

The results of studying reflectivity or reflection losses are reported for

(i) aluminum-coated carbon-fiber-reinforced-plastic (CFRP) antenna reflectors for cooled-receiver radiotelescopes ("Plank," "Hershel," ALMA, and "Millimetron"), as well as "hot" antennas for artificial Mercurian satellites ("Bepy Colombo" project);

(ii) minimal-loss mirrors for high-power transmission lines and various metals and alloys with different protective coatings.

A special section is allocated for resonator methods of measuring atmospheric absorption, in particular, continuum absorption by water vapor.

2. INSTRUMENTATION

Various types of the classical open Fabry–Perot resonator with Q-factors about 10^6 are used to study gases and condensed media. The refractive index and losses are derived from the measured resonance

* trt@appl.sci-nnov.ru

Institute of Applied Physics of the Russian Academy of Sciences, Nizhny Novgorod, Russia. Translated from Izvestiya Vysshikh Uchebnykh Zavedenii, Radiofizika, Vol. 52, No. 8, pp. 583–594, August 2009. Original article submitted June 23, 2009; accepted August 25, 2009.

0033-8443/09/5208-0525

central frequencies and widths of idle and loaded resonator. Since the Q-factor is very high and the frequency measurements are the most accurate and robust, record high sensitivity and precision are achieved using such instrumentation. Hence, the main efforts are aimed at developing measurement techniques in which all measured quantities are frequencies. Since the resonator facility (resonator spectrometer) and its pros are described in detail in [1–4], this paper is focused on the main features by which the achieved accuracy and sensitivity are over an order of magnitude better in comparison with world analogs.

The spectrometer comprises radiation sources (backward-wave oscillators) with high-precision digital frequency-control system based on a phase-locked loop using a harmonic of computer-controlled synthesizer with a reference quantum frequency standard. The resonance-curve profile is measured using a system of rapid frequency scanning employing a phase-locked loop which ensures continuous-phase switching. Lorenzian profile is fitted to each record, the corresponding width is determined, and then the resonance widths are averaged. Upon averaging of about 500 double-pass scans, the accuracy of resonance-curve measurement reaches 20 Hz for a resonance width of about 200 kHz. This corresponds to an absorption sensitivity for gases of about 0.001 dB/km. The same accuracy for a 1-mm thick dielectric plate corresponds to $\tan\delta \sim 10^{-7}$. This sensitivity of the facility is sufficient to analyze all modern dielectrics including micron films and is more than an order of magnitude higher than the sensitivities of known spectrometers [3].

The resonator is placed into a dry-nitrogen-filled chamber to eliminate the influence of atmospheric inhomogeneities during high- and low-temperature measurements and during the handling time in measurements of ultralow-loss samples.

3. MEASURING THE DIELECTRIC PARAMETERS

To calculate the refractive index n and loss tangent $\tan\delta$ of a plane-parallel dielectric plate (including liquid dielectrics), we developed a technique excluding mechanical measurements of the plate thickness which is also calculated using the results of microwave measurements. The experiments are carried out using resonance frequencies for which the plate thickness is equal to an even number of half-waves. Thus, the main error of refractive-index measurement due to mechanical determination of the dielectric thickness is eliminated [1].

The value of $\tan\delta$ is calculated using the measured resonance-curve widths of the idle resonator and resonator with a plate whose planes are located at the maximum and minimum electric field of the standing wave in the resonator. The loss tangent $\tan\delta$ is calculated using three pairs of measured line widths, so that the measurement results can additionally be verified since all three calculations should yield identical results [5].

Another key aspect is the possibility to avoid measuring the idle-resonator Q-factor by determining $\tan\delta$ for two positions of the plate. In other words, it is not necessary to measure the idle-resonator Q-factor, i.e., it is not necessary to extract the studied sample from the resonator. It is fairly convenient to study temperature dependences of $\tan\delta$ by placing the studied sample in heating or cooling fitting inside the resonator [6].

An important outcome of measuring the absorption for two positions of the plate and taking into account information on idle-resonator losses makes it possible to detect a thin enhanced-loss surface layer whose thickness is much less than the wavelength λ and to calculate the absorption in such a layer [5].

Table 1 lists the parameters of dielectrics widely used in the microwave band [7, 8]. The spread of n and $\tan\delta$ values corresponds to the maximal and minimal measured quantities in a series of samples. The four-digit values are returned by measurements of n for single samples. Note that the majority of materials show insignificant scatter of the refractive-index values in the millimeter- and submillimeter-wave ranges, while the value of $\tan\delta$ is approximately proportional to the frequency and is extrapolated to zero for the zero frequency. For materials with conductivity-dominated absorption such as semiconductors, some types of glasses, and composites, the loss tangent $\tan\delta$ is inversely proportional to the frequency for up to about 1 THz. Correspondingly, dielectrics with absorption of mixed type have complex frequency and temperature dependences of $\tan\delta$.

TABLE 1. General-purpose materials.

Material		n	$10^4 \tan\delta$	f, GHz
Pyrolytic boron nitride (BN)		2.1−2.2	8−18	140
Hot-pressing boron nitride		1.78−1.79	14−15	140
AlN		2.89−2.91	23−38	146
		2.914	6.5−6.4	170
BeO		2.60−2.62	8−10	165
LiF		3.0	7.6	140
CaF		2.610	20	150
Crystalline quartz	n_o	2.108	0.5−0.9	140
	n_e	2.155	0.24−1.80	140
Quartz glass (SiO_2)	KU grade	1.958	14−15	150
	KV grade	1.953−1.952	5.9−7.1	150
	KI grade	1.952	5.0−5.3	150
Quartz glass (single sample)		1.949	4.2	160
Leucosapphire (Al_2O_3 crystal)	n_o	3.066−3.071	2.1−2.5	150
	n_e	3.400−3.405	1.1−1.5	150
Sapphire ceramics (pure Al_2O_3)		3.244−3.252	2.7−3.2	140
22XC		3.05−3.06	30−35	140
Mica of ST grade		2.543	18	155

Table 2 lists the parameters of modern polymer materials. Note the low losses of the polyethylene produced by "Kazanorgsintez" PLC in the form of thick plates and sheets with a thickness of about 1 mm. In the case of foam plastic, the field component scattered by air bubbles and the refractive-index gradient over the sheet thickness are fairly large. For example, the parameters of a plate cut from the outer layers of PS-1-150 correspond to the inner layers of PS-1-200, etc. Note also that n is fairly anisotropic in mutually orthogonal directions.

Techniques and results of measuring the parameters of films are reported in a special paper [9]. Note that rolled films have significant polarization anisotropy of the electric field **E** along and across the roll. In general, all three refractive-index components are nonzero. Only one of the widely used materials, polyamide film, did not show the polarization effects. Another issue refers to variations in the parameters due to volumetric and surface adsorption of water by a film. The film parameters at room temperature are almost linear functions of the humidity up to 70%. Polyamide shows the strongest humidity dependence of n and $\tan\delta$. Adsorption of water by Teflon films was not observed for the current sensitivity of the spectrometer.

Table 3 shows the most interesting results for the best samples of semiconductor materials. A series of experiments were carried out to study dielectric losses in state-of-the-art chemical-vapor-deposition (CVD) diamonds and single-crystal silicon [10] at frequencies 45–350 GHz and temperatures 20–650 °T. It was found that the losses in CVD diamonds at frequencies of up to 180 GHz are mainly related to the extrinsic conductivity ($\tan\delta \sim 1/f$ decreases with increasing frequency) [5, 6, 11, 12]. "Unstable" behavior of samples with $\tan\delta \sim 10^{-5}$ and even $\tan\delta \sim 10^{-6}$ was discovered at frequencies above 200 GHz. It was found that $\tan\delta$ increases with increasing frequency (Fig. 1). The calculations [13] showed that this apparent increase in losses is related to scattering by structural irregularities of the CVD-diamond polycrystal, namely scattering by voids between crystallites. However, about 70–80% of the scattered energy is absorbed in the CVD-diamond volume. This should be taken into account when using CVD-diamonds at frequencies above 200 GHz.

The loss tangent $\tan\delta$ of single-crystal gold-compensated silicon [10] is exactly inversely proportional to the frequency, i.e., no lattice component of the losses is found. The losses are dominated by the conduc-

TABLE 2. Polymer materials.

Polymers	n	$10^4 \tan\delta$	f, GHz
Teflon	1.400−1.415	3−4	50−200
Teflon film	1.51		100−200
Low-pressure polyethylene 271-274K ("Kazanorgsintez" PLC)	1.527−1.530	3.5−3.6	100
Polyethylene 153-02K	1.5109	3.2	150
("Kazanorgsintez" PLC, GOST 16 336-77)	1.5100	3.1	113
MEKAPOL	1.54	22	140
Iroplact	1.59	15−20	140−200
Foam plastics			
PS-1-150	1.18	25	155
PS-1-200	1.22	35	155
PS-1-350 $\parallel$	1.28	40	155
PS-1-350 $\perp$	1.29	40	155
Liquid dielectrics			
Perfluorodibutyl ether $(C_4F_9)_2O$	1.3469	30	146
Fluorinert FC-75	1.3445	24	146
Nonane C_9H_{20}	1.4010	10	146

TABLE 3. Semiconductors.

Semiconductors	n	$10^4 \tan\delta$	f, GHz
CVD diamond (T)	2.38	up to 0.02	200−300
Silicon, $\rho \sim 40\,\mathrm{k\Omega\cdot cm}$ (Si)	3.418−3.423	0.1	130−170
Gold-doped silicon	3.418−3.423	up to 0.01	200−300
Silicon carbide with 6= structure (SiC)	3.14−3.16	0.2−0.4	140
Cubic boron nitride (BN)	2.657	12	150
Gallium phosphide (GaP)	3.355	2.3	100−200
Gallium arsenide (GaAs)	3.600	3.5	210
	3.591	2.8	120
	3.593	3.3	200
Indium phosphide (InP)	3.34	4.9	100
	3.43	4.6	200
Zinc selenide (ZnSe)	3.015	20	100−200

tivity due to free carriers. No features of absorption are expected at least up to a frequency of 1 THz. At present, silicon of this type has the minimum losses among all materials.

The analytical formulas derived in [11] for $\tan\delta$ of CVD diamonds imply that there is a possibility for decreasing losses by at least one order of magnitude. Figure 2 presents typical temperature dependences of n, $\tan\delta$, and the resonance frequency for CVD-diamond windows with a thickness of about 1.8 mm produced by "De Bears" company. In fact, we show all the parameters necessary to calculate the temperature regime of a megawatt-gyrotron output window. The temperature dependence of $\tan\delta$ is smooth and does not show linear segments in the Arrenius coordinates. This implies the presence of a variety of impurities with different ionization energies in the studied diamond [11, 12].

Table 4 presents the dielectric parameters of ferrites for the microwave band. Ferrites are multi-component sintered materials whose refractive indices and losses show significant scatter even for various samples of the same grade. The table shows the extreme values measured for a series of 30Sch3 samples manufactured by different companies.

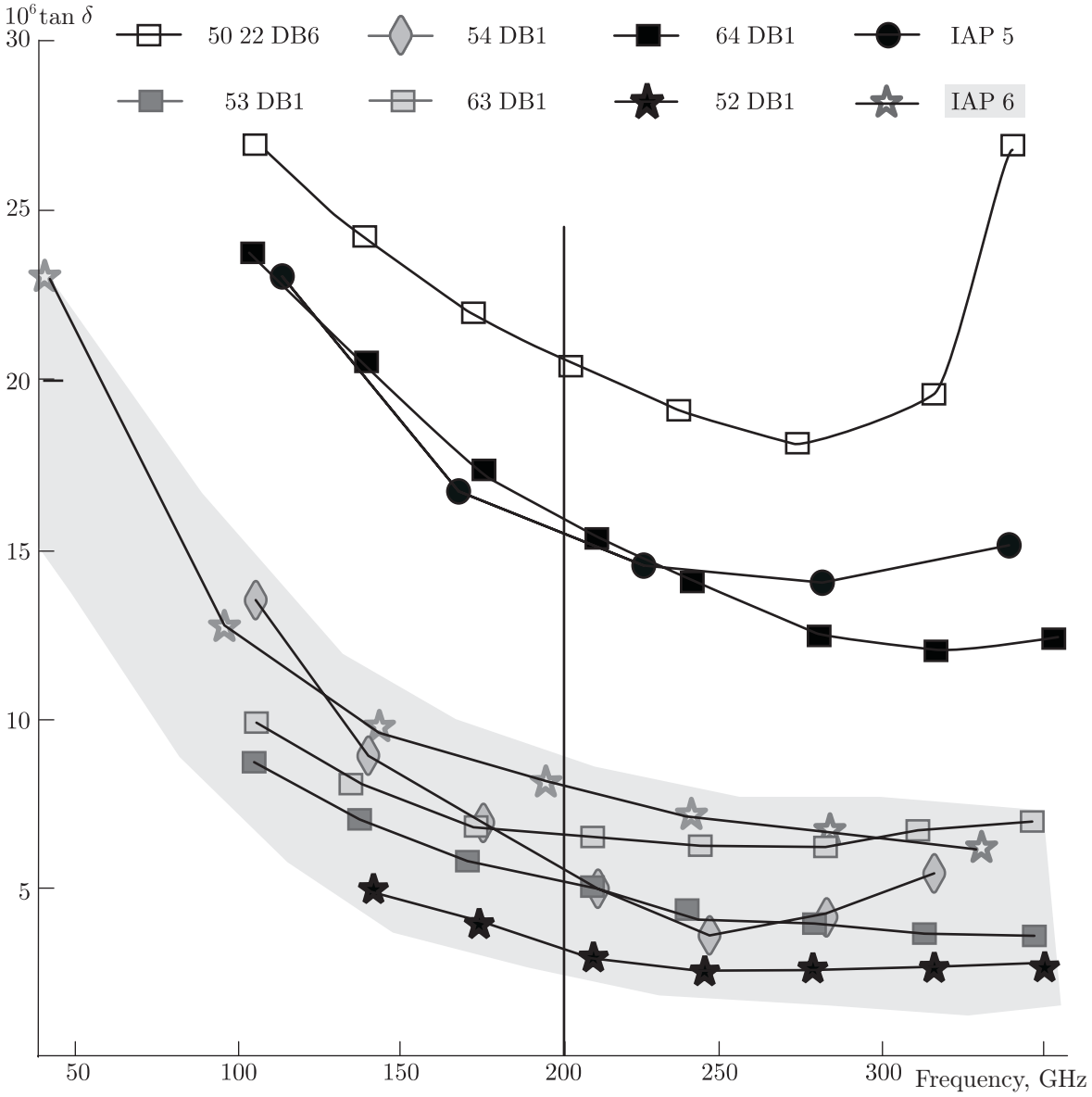

Fig. 1. Frequency dependences of losses for CVD-diamond windows produced by "De Bears" company (the DB mark) and the Institute of Applied Physics (the IAP mark).

Table 5 lists the dielectric parameters of lithium niobate, a popular material for optical-flux modulation. Note that lithium niobate has a tremendously high refractive index in the millimeter-wave range and fairly low losses.

4. STUDYING REFLECTION LOSSES

A relatively new field of using the resonance spectrometer is studying reflection losses in the case of reflection from ultrapure metals and actual metals and alloys. Three following lines of research can be mentioned:

1) development of resonator mirrors with minimal return losses;

2) studying coatings for ground-based and spaceborne antennas ("Planck," "Hershel," ALMA, "Millimetron," and "Bepy Colombo" projects);

3) development and study of mirrors for high-power transmission lines.

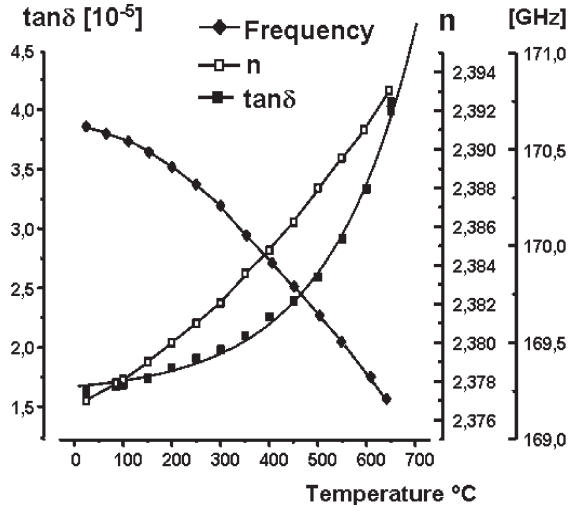

Fig. 2. High-temperature dependences of n, $\tan\delta$, and the resonance frequency for a CVD-diamond window of the standard thickness 1.8 mm [5].

No features are known for frequency dependences of return losses of "perfect"-surface metals at frequencies of up to a few terahertz. The frequency dependence of losses is fitted well with a function of the form $1 - R = 2\sqrt{f/\sigma}$, where R is the reflectivity, f is the frequency, and σ is the dc conductivity. A feature of the microwave band is that the skin depth can be both less and greater than the typical roughness size resulting from conventional mechanical and chemical processing technologies (see Table 6), while the losses can be almost doubled due merely to surface roughness [14]. In addition, any surface finishing modifies this thin reflecting layer, so there is significant (by a factor of few) dependence of the reflection losses on the surface-finishing technology, type of oxidation, protective surface coating(s), etc. In summary, it is impossible to calculate the reflection losses with fairly good accuracy based on only the dc conductivity. The case of multilayer coating is even more complicated.

4.1. Best-reflectivity mirrors (the first four metals in Table 6)

Only a mirror made of high-purity (0.99996) aluminum surface finished by diamond tool [15] ($R_a \sim$ 30 nm) has reflection losses only 1.5% above the calculated value. The best result for a gold coating was

TABLE 4. Ferrites.

Ferrite grade	n	$10^3 \tan\delta$	f, GHz
30Sch3	3.503−3.530	1.7−3.6	150
10Sch6	3.901	1.4	150
10Sch3	3.072	2.5	150

TABLE 5. Lithium niobate ($LiNbO_3$).

	n	$10^3 \tan\delta$	f, GHz
Z-cut ($\mathbf{E} \perp \mathbf{Z}$)	5.0	5	120
	5.7	6	200
Y-cut ($\mathbf{E} \parallel \mathbf{X}$)	6.664	3.5	100
		7.0	180
Y-cut ($\mathbf{E} \parallel \mathbf{Z}$)	5.064	5.0	100
		7.5	190

TABLE 6.

Surface finish class (from 14 to 6) and arithmetic mean deviation R_a									
Surface finish class	14	13	12	11	10	9	8	7	6
R_a, μm	0.01	0.02	0.04	0.08	0.16	0.32	0.64	1.3	2.6

Skin depth δ at a frequency of 100 GHz													
material	Ag	Cu	Au	Al	Be	Rh	W	Mo	Zn	Ni	LS-59	Cr	Ti
δ, μm	0.20	0.21	0.25	0.27	0.32	0.34	0.36	0.37	0.39	0.44	0.45	0.65	1.1
Calculated losses for a frequency of 100 GHz													
$10^3\,(1-R)$	0.85	0.87	1.00	1.11	1.34	1.46	1.50	1.55	1.63	1.78	1.81	2.72	4.6

obtained for a galvanic 2.8-μm layer manufactured according to the technology developed at the Federal State Unitary Science and Industrial Enterprize "Salyut" (Nizhny Novgorod, Russia). Reflectivity losses for this coating is only 20% above the theoretical figures. All other gold coatings including vacuum-deposited have higher losses. In the case of conventional oxygen-free copper (0.9928 purity) surface finished by a diamond tool ($R_a \sim 20$ nm), the losses are 8–10% above the calculated values. The best reflector today is a vacuum-deposited 1-μm silver layer protected from oxidation by a 10-μm aluminum-oxide layer. Its losses are only 8–10% and stable in time [16].

4.2. Antennas for space-borne and ground-based radiotelescopes

Special attention to reflectivity studies is fueled by the development of satellite-borne and ground-based millimeter- and submillimeter-wave telescopes with high-sensitivity receivers cooled to 0.1 K with helium III. In this case, antenna losses or, in other words, its own emission, significantly increase the receiver noise temperature. For example, if $T = 300$ K and $1 - R = 0.001$, each reflection adds 0.3 K to the noise temperature per reflection. Since a typical circuit comprises at least three reflectors, we arrive at about 1 K of the added unstable noise temperature. In reality, the values are one order of magnitude greater. Special attention is paid to decreasing reflection losses since, e.g., it is announced that the "Planck" and "Hershel" missions should be able to measure anisotropy of the cosmic microwave background at the level $\Delta T/T \sim 10^{-6}$ and even detect polarization anisotropy.

At present, carbon fiber-reinforced plastic (CFRP) is the most popular ultra-light material for millimeter- and submillimeter-wave antennas. However, its reflection losses are $3 - 4\%$ and about 30% for the field **E** directed along and across the fibers, respectively, which is absolutely unacceptable. Hence, the reflecting CFRP surface is coated by metal. In most cases, thin aluminum layers on a polymer film glued to the carbon fiber-reinforced plastic are used. Such a film also protects aluminum from oxidation and total disappearance. However, studies of CFRP coatings [15–17] showed that even the reflectors cooled down to 80 K have losses a few times greater than the calculated values. This results in a significant increase in the noise temperature of cryogenic high-sensitivity receivers.

"Hot" antennas for artificial Mercurian satellites were tested within the framework of the "Bepy Colombo" project. Five titanium-alloy (Ti6Al14V) samples with reflecting surfaces subjected to different treatment technologies ($R_a = 0.02$–0.4 μm) were studied at frequencies 65–160 GHz. The reflection losses for all these samples are almost identical and close to the calculated values. The difference is less than 1.5% in the entire frequency and temperature ranges, so that the surface-finishing technology has almost no effect on such high losses (see Table 7). Studies of the temperature behavior of losses by heating samples up to 500 °C in dry nitrogen and air did not reveal any variations in the reflection losses despite the clearly observed obvious nitridation and oxidation of the surfaces. The reflection losses of a pure-aluminum mirror (0.99994 purity) correspond to the calculated values in the entire measurement range and at temperatures from 80 to 500 K in air and nitrogen. The oxide film (Al_2O_3) perfectly protects the metal from oxidation at up to the melting temperature [15].

4.3. Mirrors for high-power transmission lines

The unit power of many high-power electronic devices is limited by the heat-sink capability of metals heated as a result of exposure to microwave radiation. For example, modern resonators, collectors, and mirrors of high-power millimeter-wave gyrotrons are already operated under conditions of ultimate heat sink from the unit surface area. The best heat and electric conductors such as copper and silver have become the main structural materials in the microwave electronics long ago. Thus, decreasing the reflection losses by appropriate surface finishing or applying high-reflectivity coating onto stainless steel, brass, etc. is a topical problem of the millimeter- and, especially, submillimeter-wave high-power electronics. For example, 25 1-MW gyrotrons and the corresponding transmission lines with 150 mirrors are planned to be used in the ITER project. Hence, technologies for electrodeposition of coatings onto the surfaces of complex-shape

TABLE 7. Reflection losses of metals at a frequency of 140 GHz.

Material	R_a, μm	Reflection losses, $10^5\,(1-R)$	
		Measurements	Calculations
LS-59 + electrodeposited silver (5-μm layer)	0.34	135	100
Copper + electrodeposited silver (5-μm layer)	0.40	135	100
LS-59 + electrodeposited silver, densed	0.80	127	100
Copper + electrodeposited silver, densed	0.57	137	100
LS-59 + vacuum-deposited silver (1-μm layer) + + Al_2O_3 (10-nm layer)	0.02	110	100
LS-59 + sulfurous coppering	0.48	130	103
LS-59	0.06	300	215
Chemically aged brass LS-59	0.47	350	215
Chromium copper	0.06	170	—
Copper (purity 0.999)	0.07	121	103
Copper (purity 0.999)	0.13	152	103
Copper (purity 0.99)	0.05	122	103
Copper (purity 0.99)	0.13	153	103
Copper (crude treatment)	3.00	160	103
Oxygen-free copper, diamond-tool finishing	0.06	120	103
Oxygen-free copper, diamond-tool finishing	2.30	125	103
Oxygen-free copper, diamond-tool finishing	0.02	110	103
Copper, vacuum deposition on glass	0.01	125	103
12-18=10T	0.06	675	670
12-18=10T	0.17	720	670
Aluminum (0.9999 purity), vacuum deposition	0.01	150	130
Aluminum (0.99996 purity), diamond-tool finishing	0.03	128	130
-16T	0.06	200	150
Titanium (0.99 purity)	0.05	620	544
Titanium (0.99 purity)	0.07	640	544
Titanium (0.99 purity)	2.55	650	544
Alloy of 80% Ti, 6% Al, and 14% V (Ti6Al14V)	0.02−0.40	1080	1100

mirrors for high-power transmission lines were developed, which ensured the resulting losses to be only 20% above the calculated values (see Table 7).

5. ATMOSPHERIC STUDIES

Millimeter- and, especially, submillimeter-wave propagation in the troposphere is mainly determined by oxygen and water vapor. In addition to the resonance absorption by molecular oxygen (fine-structure and rotational transitions) and in rotational water lines, there is also nonresonance, the so-called continuum absorption whose physical nature is not yet fully understood (absorption by molecular complexes, collision-induced absorption, etc. are discussed).

Development of precision models of millimeter- and submillimeter-wave absorption under various meteorologic parameters such as pressure, temperature, and humidity requires precise information on the parameters of resonant molecular absorption lines as well as non-resonant (or continuum) absorption. It is impossible to get such information using open-air paths since meteorological conditions are uncontrollable. However, measurable absorption in weak lines or continuum absorption in transparency windows can only be

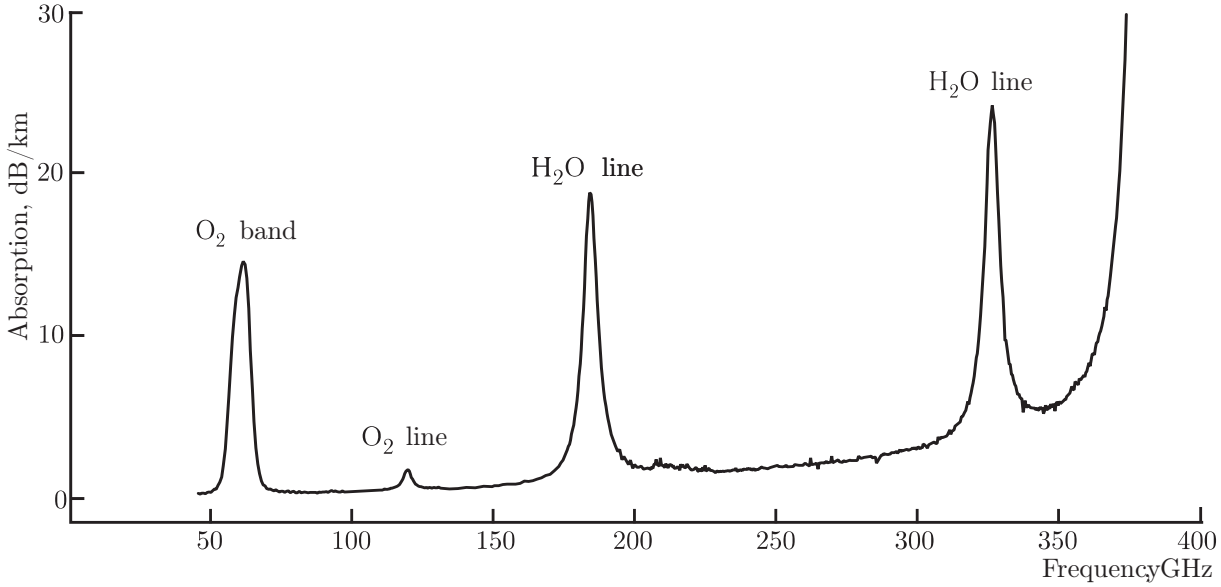

Fig. 3. Wideband record of the atmospheric air absorption for a humidity of 5.3 g/m^3, a pressure of 730 Torr, and a temperature of 298.3 K [23].

obtained using large path lengths. Hence, high-Q Fabry–Perot resonators with huge effective path lengths are used for high-precision measurements of the atmospheric absorption [2, 3, 18–20].

The 500-mm long resonator used in our spectrometer has an effective path length of about 1 km. The resonator is placed into a chamber with well-controlled parameters of studied gases. In particular, gas temperature can be set from -30 up to +60 °C with accuracy of 0.2 °C and humidity from 0 to 90% of relative humidity. Thus, contrary to long-path field measurements, the spectrometer allows one to study gas absorption using long paths with well-controlled conditions.

Figure 3 presents a wideband (45–370 GHz) record of atmospheric air absorption spectrum obtained by the resonator spectrometer at room temperature and atmospheric pressure (see review paper [23] and references therein). Within this frequency range, the following spectral features were studied with highest (up to date) sensitivity: water vapor absorption lines at 183 [23] and 325 [22] GHz, oxygen absorption line at 118 GHz [24], and oxygen absorption band at 60 GHz [25]. The following line parameters were determined with high accuracy: nitrogen and oxygen pressure broadening parameters, integral intensities, oxygen, nitrogen and dry air pressure shifts of line center frequencies, and collisional coupling parameters of the oxygen fine structure. Also, the shape of the 60-GHz oxygen absorption band profile at atmospheric pressure was refined. The results of these studies obtained at atmospheric pressure are in good agreement with the results obtained at low (from 1 to 5 Torr) pressures by the spectrometer with radioacoustic detection of absorption (RAD spectrometer) [23] operated in the same frequency range. The performed studies resulted in increased accuracy of calibration of atmospheric absorption in the millimeter and submillimeter radiation propagation models [23].

One of the problems to solve with the use of the resonator spectrometer is study of the humidity-related continuum absorption [26]. For this purpose, we implemented a resonator scheme of the path length variation method, in which an assembly of two resonators, symmetric and half-length semi-symmetric, is used [21]. Results of the preliminary studies of continuum absorption in a broad range of temperatures and pressures [21] show that water absorbed at the resonator elements (mirrors and coupling films) introduces a significant error in the value of the sample absorption. It should be mentioned that the results of all previous studies of the continuum absorption performed by other researchers (see references in [21]) include, to a certain extent, this systematic error. The implementation of a two-resonator module in our spectrometer permits direct measurement of the humidity-related radiation loss in the resonator elements, which minimizes systematic errors in the determined value of the continuum absorption. In a long-lasting history of continuum

research, this method was employed for the first time [21].

High accuracy of measured parameters of water vapor resonance lines and record characteristics of the spectrometer allows its use as a precision meter of volumetric sample humidity in real time under atmospheric conditions. The estimated water vapor content sensitivity is about 10 mg/m^3 if a 183-GHz water absorption line is used and $2{\cdot}10^{-2}$ mg/m^3 if a 556-GHz line is used.

REFERENCES

1. Yu. A. Dryagin and V. V. Parshin, *Int. J. Infrared Millimeter Waves*, **13**, No. 7, 1023 (1992).
2. A. F. Krupnov, V. V. Parshin, M. Yu. Tretyakov, et al., *Int. J. Infrared Millimeter Waves*, **20**, No. 10, 1731 (1999).
3. A. F. Krupnov, M. Yu. Tretyakov, V. V. Parshin, et al., *J. Mol. Spectrosc.*, **202**, 107 (2000).
4. M. Yu. Tretyakov, V. V. Parshin, M. A. Koshelev, et al., *J. Mol. Spectrosc.*, **238**, 126 (2006).
5. E. V. Koposova, S. E. Myasnikova, V. V. Parshin, et al., *Diamond Rel. Mater.*, **11/8**, 1485 (2002).
6. V. V. Parshin, B. M. Garin, S. E. Myasnikova, et al., *Radiophys. Quantum Electron.*, **47**, No. 12, 574 (2004).
7. V. V. Parshin, *Int. J. Infrared Millimeter Waves*, **15**, No. 2, 339 (1994).
8. V. V. Parshin, "Dielectric materials for gyrotron output windows," Preprint No. 342 [in Russian], Institute of Applied Physics, Nizhny Novgorod (1993).
9. S. N. Vlasov, V. V. Parshin, and E. A. Serov, *Radiophys. Quantum Electron.* [in press].
10. V. V. Parshin, R. Heidinger, B. A. Andreev, et al., *Int. J. Infrared Millimeter Waves*, **16**, No. 5, 863 (1995).
11. B. M. Garin, V. V. Parshin, S. E. Myasnikova, et al., *Diamond Rel. Mater.*, **12**, Nos. 10–11, 1755 (2003).
12. B. M. Garin, V. I. Polyakov, V. V. Parshin, et al., *Diamond Rel. Mater.*, **15**, Nos. 11–12, 1917 (2006).
13. O. S. Mocheneva and V. V. Parshin, *Radiophys. Quantum Electron.*, **50**, No. 12, 946 (2007).
14. S. E. Myasnikova, C. G. M. van't Klooster, and V. V. Parshin, in: *Proc. 3rd ESA Workshop on Millimeter Wave Technology and Applications, Finland, 2003*, p. 15.
15. V. Parshin, E. Serov, C. G. M. van't Klooster, et al., in: *Proc. 5th ESA Workshop on Millimeter Wave Technology and Applications and 31st ESA Antenna Workshop, ESTEC, The Netherlands, 2009*, p. 593.
16. V. V. Parshin, in: *Proc. 6th Int. Conf. Antenna Theory and Techniques (ICATT'07), Sevastopol, Crimea, 2007*, p. 71.
17. V. Parshin, C. G. M. van't Klooster, and E. A. Serov, in: *Proc. 30th ESA Antenna Workshop on Antennas for Earth Observation, Science, Telecommunication and Navigation Space Missions, ESA/ESTEC, Noordwijk, The Netherlands, 2008*, p. 353.
18. H. J. Liebe, G. A. Hufford, and M. G. Cotton, in: *AGARD Conf. Proc.*, **542**, 3 (1993).
19. T. Kuhn, A. Bauer, M. Godon, S. Buhler, et al., *J. Quant. Spectr. Radiat. Transfer*, **74**, 545 (2002).
20. A. I. Meshkov and F. C. De Lucia, *Rev. Sci. Instr.*, **76**, 83 (2005).
21. M. Yu. Tretyakov, A. F. Krupnov, M. A. Koshelev, et al., *Rev. Sci. Instr.*, **80**, No. 9, 093106 (2009).
22. M. A. Koshelev, M. Yu. Tretyakov, G. Yu. Golubyatnikov, et al., *J. Mol. Spectrosc.*, **241**, 101 (2007).
23. M. Yu. Tretyakov, G. Yu. Golubyatnikov, V. V. Parshin, et al., *Radiophys. Quantum Electron.*, **51**, No. 9, 713 (2008).
24. M. Yu. Tretyakov, G. Yu. Golubyatnikov, V. V. Parshin, et al., *J. Mol. Spectrosc.*, **223**, No. 1, 31 (2004).

25. M. Yu. Tretyakov, M. A. Koshelev, V. V. Dorovskikh, et al., *J. Mol. Spectrosc.*, **231**, No. 1, 1 (2005).
26. M. Yu. Tretyakov, M. A. Koshelev, I. A. Koval, et al., *Opt. Atmos. Okeana*, **20**, No. 2, 101 (2007).